Forecasting Research

Forecasting Research Division
Technical Report No. 229

An initial assessment of parameters derived from SSM/I data with a 1DVAR scheme

by

J K Ridley and G E Holpin

December 1997

Meteorological Office
London Road
Bracknell
Berkshire
RG12 2SZ
United Kingdom

Forecasting Research
Technical Report No. 229

An initial assessment of parameters derived from SSM/I data with a 1DVAR scheme

by

J K Ridley and G E Holpin

December 1997

Forecasting Research
Meteorological Office
London Road
Bracknell
Berkshire
RG12 2SZ
United Kingdom

© Crown Copyright 1997

Permission to quote from this paper should be obtained from the above Meteorological Office division.

Forecasting Research Division
Technical Report No. 229

An initial assessment of parameters derived from SSM/I data with a 1DVAR scheme

by

J K Ridley & G E Holpin

(December 1997)

Abstract

A 1DVAR scheme, applied to SSM/I data, has been implemented on the Met office's UNIX workstations and a preliminary assessment of the scheme has been conducted. Results from the scheme have been compared with those from standard SSM/I regression algorithms and with background fields, from the Unified Model (UM), to assess the likely benefit of assimilating the 1DVAR products into the UM. The products assessed are total precipitable water, cloud liquid water and surface wind speed.

Contents

1. Introduction 1
    1.1 The SSM/I instrument 1
    1.2 Traditional retrieval techniques 2
    1.3 The variational approach 3
    1.4 Variational theory 3

2. SSM/I 1DVAR Proceedures at the Met. Office. 4
    2.1 The routine acquisition of global SSM/I data
        by the UK Met office 4
    2.2 Development of the SSM/I 1DVAR software 4
    2.3 Parallel assimilation trials on Cray T3E 5

3. Initial Case Study 5
    3.1 Total Precipitable Water (TPW) 5
    3.2 Surface Windspeed 6
    3.3 Cloud Liquid Water (CLW) 6

4. Areas for Improvement 7
    4.1 Incidence angle 7
    4.2 Azimuth Angle 8
    4.3 Sea ice edge 8
    4.4 Data thinning 8

5. Conclusions 8

6. References 9

7. Figure Captions 11

Appendices 12
    APPENDIX A: SSM/I Fields stored in MetDB 12
    APPENDIX B: SSM/I biases 14
    APPENDIX C: Output Parameters 15

1. Introduction

1.1 The SSM/I instrument.

The Special Sensor Microwave Imager (SSM/I) is a seven channel microwave imager on-board the U.S. DMSP (Defence Meteorological Satellite Program) satellite series. The SSM/I instrument operates at frequencies of 19.35, 22.235, 37 and 85.5 GHz in both horizontal (H) and vertical (V) polarizations (except 22.235 GHz which measures vertical polarization only). The instrument has a conical scan with a surface incidence angle of 53.1 degrees and a 1400 km swath, giving effective fields of view (spatial resolutions) of 69 by 43 km (19 GHz channel), 60 by 40 km (22 GHz channel), 37 by 28 (37 GHz channel) and 15 by 13 km (85 GHz channel). The SSM/I scanning geometry is shown in Figure 1.

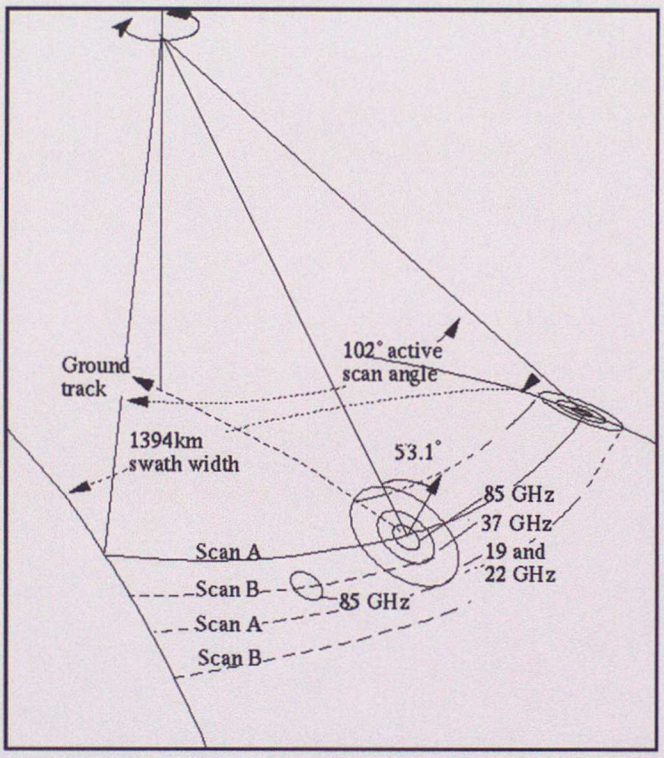

Figure 1. SSM/I scanning geometry (from Hollinger et al. 1990)

The SSM/I orbit is near-circular, sun-synchronous, and near-polar, with an altitude of 860km and inclination of 98.8 degrees. The 102 minuite orbit provides near daily global coverage at the equator.

Satellite	Launch date	Equator crossing time (local time)
F-10	01/12/90	~00:00 (drifting orbit)
F-11	28/11/91	18:25
F-13	24/03/95	17:43
F-14	04/04/97	20:15

Table 1. The currently operational SSM/I satellites

Lying in the microwave region of the spectrum, the SSM/I channels are sensitive (to varying degrees, depending on channel and atmospheric conditions), to both atmospheric and surface parameters. For this reason it has been found possible to derive from SSM/I data both surface characteristics, such as sea ice cover and sea surface wind speed, and atmospheric parameters, such as total precipitable water vapour (TPW) and total column cloud liquid water (CLW). It is worth noting that the SSM/I instrument is a scanner, giving only column total quantities without any vertical structure information such as that given by atmospheric sounding instruments.

1.2 Traditional retrieval techniques.

The measurement of water parameters from space is of great interest, due to the importance of water in meteorological processes. Microwave remote sensing techniques are well suited to measuring these water parameters as microwaves are able to penetrate clouds and the instruments therefore receive radiation emitted throughout the depths of the cloud - unlike VIS and IR sensors. They also have the property that if no precipitation is present in the field of view, little scattering occurs and the radiative transfer processes are straightforward and generally well understood.

Different SSM/I frequencies and polarizations respond to the various surface and atmospheric parameters in different ways. Since the launch of the DMSP series, the traditional approach has been to develop regression algorithms which use combinations of the various channels along with available a priori information in an attempt to retrieve the required surface or atmospheric variables. Many algorithms have been developed and are widely reported in the literature. A description of the most commonly used algorithms can be found in Deblonde and Wagneur (1997).

In addition to the above parameters, regression algorithms for SSM/I are routinely used to derive sea ice extent and concentration (eg. Steffen and Schweiger, 1991) and snow cover depth (eg. Nagler and Rott, 1992). Under certain circumstances SSM/I can also be used to derive precipitation rates (eg. Sheu et al., 1996) and soil moisture (eg. Teng et al., 1993; Jackson, 1997). However, these surface parameters are not the subject of the current work and will not be discussed further.

An example of the liquid water path (CLW) generated from SSM/I data using a simple statistically based algorithm developed by Alishouse et al. (1990) is shown in Figure 2. Initial experiments with the assimilation of these SSM/I derived quantities into Numerical Weather Prediction (NWP) models have shown encouraging results, with positive benefits to the forecast cycle (eg. Ledvina and Pfaendtner, 1995).

However, although many regression techniques have been shown to work well at deriving the required physical parameters in 'simple' atmospheric conditions (especially clear sky), they generally all suffer from the fact that they over-simplify the retrieval problem, and usually do not have the benefit of high quality *a priori* information available to them. The non-linearity of the retrieval problem becomes particularly acute when clouds, ice or precipitation sized particles are present in the SSM/I field of view (*eg.* Bauer and Schluessel, 1993).

1.3 The variational approach.

A different approach to the extraction of useful information from SSM/I data, and one which is being adopted increasingly is that of optimal estimation (Rodgers, 1976). In this method, the required physical parameters are estimated simultaneously and are the best set of parameters which explain the observed SSM/I brightness temperatures (top of atmosphere radiances). A great advantage of this variational approach is that it allows the retrieval to take place whilst keeping the derived atmospheric profile consistent with high quality *a priori* information in the form of an NWP forecast of the atmospheric state at the time of the SSM/I data. A further advantage of this technique (from now on referred to as SSM/I 1DVAR, as it is a one-dimensional variational retrieval), is that a direct by-product of the technique is an estimate of the errors of the retrieval process.

The 1DVAR technique is currently used operationally at the European Centre for Medium Range Weather Forecasting (ECMWF) for processing the TIROS Operational Vertical Sounder (TOVS) data (Eyre, 1993) and is on the point of (as of Dec. 1997) being used operationally with SSM/I data (Phalippou, 1996). Parallel trials incorporating SSM/I 1DVAR have significantly improved the skill of the forecasts (E. Gerard, personal communication). The Canadian Meteorological Centre (CMC) have also implemented a 1DVAR scheme, which has been used to validate their analysis/forcast system. Both the CMC and ECMWF schemes show similar results to those from the UK Met. Office scheme discussed here.

1.4 Variational theory

If we define x as the state vector (control variable) formed by the atmospheric and surface variables then what we are trying to achieve is the best estimate of x, knowing the *a priori* (background) vector x_b (defined here as an NWP forecast field) and the coincident satellite observation vector y_0. We denote by $H\{x\}$ the operator mapping the control variable x into the observation (satellite) space. In the case of SSM/I 1DVAR, $H\{x\}$ is the radiative transfer model which calculates the SSM/I brightness temperatures corresponding to the control variable x. If we assume that the errors in the observations and the errors in the *a priori* information have Gaussian distibutions and are uncorrelated, then the cost (inverse of likelihood) function is given by the following:

$$J(x) = \tfrac{1}{2}(H\{x\}-y_0)^T.(O-F)^{-1}.(H\{x\} -y_0) + \tfrac{1}{2}(x-x_b)^T.B^{-1}.(x-x_b)$$

Where O is the expected error covariance of the observations, F is the expected error covariance of the radiative transfer model (the forward operator) and B is the expected error covariance of the background x_b. T denotes the transpose of a vector. Note that the two terms in the above expression represent the observation and background costs respectively. The function of SSM/I 1DVAR is therefore to minimize this expression (minimum cost) and find the best estimate of x within the given constraints. For more details see Rodgers (1976).

2. SSM/I 1DVAR Procedures at the Met. Office.

Our aim is to implement a similar scheme at the UK Met office to that currently being used at ECMWF. This section describes the current and future stages in the aquisition, 1DVAR processing and assimilation of SSM/I data.

2.1 The routine acquisition of global SSM/I data by the UK Met office

SSM/I brightness temperature data has been archived in the UK Met Office meteorological database (MetDB) since February 1997.

At present the source of the data is ECMWF whichobtains raw SSM/I data in near real time from NOAA (NESDIS) over an internet link (DMSP F-11 only). These data are then converted to BUFR format and downloaded via DECNET using ECMWF NTS software, to the UK Met Office each night. The fields in the data stream, which are stored in the MetDB, are indicated in Appendix A. A total of ~63,000 observations per hour are archived, with missing data amounting to less than 5%.

In the future, it is planned that the UK Met Office should obtain the raw SSM/I data directly from NOAA NESDIS over the ATOVS dedicated link, and that the UK Met Office will become the European distribution point for these data. SSM/I data will be pushed from the CEMSCS server at NESDIS using TCP/IP protocols. Conversion to BUFR format (for archiving) will take place in house. It is planned that data obtained in this way will be available in the MetDB by early 1998. Initially, only data from one DMSP satellite, F-14, will be sent. Once the assimilation process has been established then data from other satellites will be required and the bandwidth of the NESDIS link will need to be upgraded to accommodate this. In addition, unlike the case of ATOVS for which a memorandum of agreement exists, there is currently no obligation on NESDIS to transmit the SSM/I data. If SSM/I assimilation is made operational the current voluntary agreement may have to be upgraded.

2.2 Development of the SSM/I 1DVAR software

A version of the SSM/I software, written by L.Phalippou at ECMWF, was obtained in early 1996. This code has now been installed on the NWP HP system, after major problems associated with the move from the ECMWF mainframe computer to the NWP workstation platform. There was also a substantial amount of work required in altering the software to use UK Met Office UM data, rather than ECMWF model data. It has been verified that the software is performing in a manner consistent with the ECMWF software. The following processing stages are undertaken:

a. SSM/I data are extracted from the MetDB on a 6 hourly cycle at times corresponding to the main model runs. Currently the code runs overnight, extracting each 6 hour period for the previous day sequentially. The extraction code, which makes use of a dedicated port to the MetDB, writes out only 1/10 of the data to file on the HP (ie. every tenth f.o.v. is selected).

b. The model fields for each run, used by 1DVAR, are extracted from the fields data base on the Cray.

c. SSM/I 1DVAR is run calling up the files from a) and b). The data are flagged for

land/cloud/rain, and parameters such as scattering index. An output file merged with the input data is produced, the parameters for which are listed in Appendix C.
d. All processing of 1DVAR output is performed using PVWave, producing images and statistics for analysis and display on the intranet.
e. PVWave files on the HP are archived and 1DVAR output files sent back to the MetDB.

A mini-project has been initiated to transfer the above processing scheme to the New-OPS. The project definition document is available at http://fr1500/~frkw/pid_ssmi_def.html

2.3 Parallel assimilation trials on Cray-T3E

An assessment of the improvement in forecast skill arising from at least 6 weeks SSM/I assimilation, will be made prior to a final decision on whether to go operational with the scheme.

3. Initial Study

A study of 5 months of data was undertaken to determine the quality of SSM/I products from 1DVAR. The identification of anomalies within the products, and an investigation thereof, was conducted through the use of global images and statistics. The global images used here illustrate the distribution of features and biases with a minimum of data averaging, consequently they are weekly means. The statistical graphs, derived from a month of observations, show the zonal mean, RMS differences of the observations from the background and the standard deviation (from the mean) of the derived parameters.

3.1 Total Precipitable Water (TPW)

The differences seen here between the Unified Model (UM) analysis and SSM/I 1DVAR are common to many models and have been reported for the ECMWF by Vesperini (1996), for the NASA/Goddard Data Assimilation System by Ledvina and Pfaendtner (1995) and for the Canadian Meteorological Centre (CMC) by Deblonde and Wagneur (1997).

The global plot of the background TPW and 1DVAR differences are shown in Figures 3a-b. The difference plot shows no poleward bias. However, there are significant differences on the westward sides of the continents, particularly the Americas, where large areas of strato-cumulous clouds form, with the background predicting 30-50% more water vapour. The background water vapour values are lower than those from 1DVAR along the ITCZ. The statistics plots in Figure 4 show that globally the TPW bias is small, at mean of 1.5%, but with an RMS difference of 17% concentrated, as expected, in the tropics and sub-tropics.

The 1DVAR retrieval compares well with the regression algorithm of Alishouse, Figure 5, with slight differences at the extremes of the water vapour values. The variability between model and 1DVAR shows some structure, as anticipated from Figure 3.

The patchy behaviour of the 1DVAR TPW excess along the ITCZ suggests some cross-talk

with cloud liquid water. However, since validation studies of SSM/I (eg. Schulz & Schluessel, 1993) have indicated that the measurement error is on the order of 1 kg m^{-2}, it seems likely that both sets of regional errors are due to a poor representation of the boundary-layer thickness in the tropics, and sub-tropics, by the model. Consequently, there can be little doubt that assimilation of TPW will significantly improve the model predictions.

3.2 Surface Windspeed

The global distribution of differences between the 1DVAR and background windspeeds is shown in Figure 6. The regions of error show little correlation with high wind speeds, and are geographically scattered. The overall statistics, Figure 7, show a small positive bias arising in the regions of the storm tracks, and a RMS difference of 1.17 m s^{-1} roughly independent of latitude.

The SSM/I winds derived from various regression algortihms have been validated by Boutin and Etcheto (1996), who find that SSM/I underestimates windspeeds, with respect to shipborne measurements (the ship windspeeds are comparable with the UM background windspeeds), by as much as 1 m s^{-1} at high windspeeds at high latitudes. Little evidence for this is found in this study. Comparing windspeeds from the Goodberlet regression algorithm with 1DVAR, Figure 8, shows that the regression results in higher windspeeds (but lower at low windspeeds), whereas 1DVAR shows little (if any) bias at high windspeeds against the background.

The wind scatterometer on ERS-1 shows a similar distribution of errors (ie. greatest across the storm tracks) but additionally shows high errors in the low windspeed regions along the ITCZ. The wind scatterometer has recently had its windspeed measurements increased by 5% which results in no net global bias with respect to the background. The RMS difference is, however, relatively large at 1.55 m s^{-1}

It is possible that the SSM/I bias is the result of cloud liquid water or ice; the latter is not currently accommodated within the 1DVAR scheme. This will be the subject of further investigation. However, a RMS windspeed difference of 1.17 m s^{-1} is not an unacceptable 'error'.

3.3 Cloud Liquid Water (CLW)

The liquid water path includes a contribution from ice, but the evaluation is highly dependent on the ice fraction determination, which is a function of temperature. Different ice-water splitting functions, can result in ice fractions varying from 0.15 to 0.9 across the temperature range 0 to -30 degrees. In addition, the global statistics of CLW can be greatly distorted depending on the rain masking algorithm used (Deblonde et al., 1997). Here the rain area mask is based on the 85GHz Grody scattering index.

The weekly mean of the background CLW, Figure 9, shows structure only for major cloud systems, while the difference plot shows very little agreement, within these localised regions, with 1DVAR. The monthly statistics in Figure 10 show no significant latitudinal biases, and a RMS difference of 30% of the mean, indicating, as expected, that the model does a poor

job with this parameter.

Comparison of the 1DVAR with the Wend CLW regression algorithm, Figure 11, shows that the two retrievals are correlated but that the estimate from 1DVAR has consistently higher values. On the other hand the 1DVAR has no correlation with the model background. In all the cases observed, and in agreement with findings by Deblonde et al. (1997), the model failed to produce any significant CLW along the ITCZ, despite having significant quantities of convective cloud depicted by the model. Since only model data coincident with SSM/I iare displayed, and since SSM/I data are filtered to remove observations of 'rain', the model data from the filtered cells are lost. It is possible that the SSM/I filter is being triggered not only by rain, but also by ice in the convective clouds, and hence all CLW along the ITCZ is being rejected making it appear that the model is failing to predict it.

Further study of the rain-masking technique to optimise the retrieval of CLW is required.

4. Areas for Improvement

4.1 Incidence angle

The incidence angles of the SSM/I radiometers on the DMSP satellites vary from satellite to satellite and exhibit variations of up to 1.5 deg during one orbit (in the case of F-10). A deviation of 1 deg from the nominal incidence angle of 53.0 deg causes brightness temperature changes of up to 2 K depending on surface and atmospheric conditions. Errors of retrieved geophysical parameters on the order of 5%-10% result when the incidence angle variation is not taken into account. This is a common property of most published statistical algorithms. For total precipitable water and cloud liquid water content the error increases with increasing parameter value. For wind speed the error is largest for low wind speed and decreases with increasing wind speed. Due to the slowly varying latitudinal dependence of the incidence angle, these errors do not cancel out when monthly means are computed.

When using the radiative transfer model, the effect of incidence angle is accommodated directly, if it is known. Unfortunately, as indicated in Appendix A, the data received via the ECMWF do not contain angular information. It is thus currently not possible to correct for the variation of angle along individual orbits. It is, however, possible to cross-calibrate different DMSP platforms through knowledge of the mean pointing angle (where this deviates from the nominal angle).

4.2 Azimuth Angle

The emissivity of the ocean surface is dependent on the angle of view with respect to the wind direction. The approximate wind direction is known *a priori* from the model, but the azimuth angle of the satellite view is not provided with the data currently transmitted from NESDIS. The brightness temperature error resulting from this omission depends on the sea state, but is on the order of 0.5 K. It is possible to reconstruct the approximate azimuth angle from spherical geometry, but with a slightly increased cost in computing overhead. It is not anticipated that wind direction will be an output from the 1DVAR process, but merely used

in initialisation.

4.3 Sea ice edge

The ice boundary is currently defined by the -1.7 °C isotherm of the sea surface temperature. This has been effective in eliminating contamination of the signal by ice pixels. A slight improvement may be made by incorporating a regression algorithm to check for ice when SST falls below 0 °C and only eliminate observations for which ice is detected.

4.4 Data thinning

The data volume is approximately 1.5 million observations a day. It is not computationally feasible to process this quantity on the HPs in real time. The current scheme is to process 1:10 of the 64 observations across each swath. The scheme used at the ECMWF is to process 1:2 observations by row and column, providing one observation per model cell. This is an effective data thinning of 1:4. A similar scheme should be adopted here when run on a supercomputer.

5. Conclusions

In assessing the performance of the 1DVAR retrieval scheme, the use of surface windspeed is a useful diagnostic tool because the retrievals are tightly constrained by the background field. In this short study it has been revealed that there are no systematic errors in the 1DVAR windspeed retrievals, but that some irregular localised biases do occur, resulting in a global mean bias above the background of +0.3 to +0.8 m s^{-1} (depending on the month). Monthly mean retrievals show that the bias is located along the ITCZ, where windspeeds are low, and broadly across the high latitude storm-tracks. It is hypothesised that these biases are either the result of VAR cross-talk from CLW or due to unmodelled scattering from cloud ice particles.

The cloud liquid water path is clearly poorly represented in the background fields, to such an extent that it bears litte relationship to the observed fields. However, the 1DVAR retrievals are biased through the requirement to filter the data for rain. The resultant field is thus highly dependent on the rain filter employed. It is also depended on the model used to define the cloud ice fraction from the cloud temperature. It may be prudent to investigate fully these matters before proceeding with the assimilation of CLW.

Total precipitable water retrievals are in agreement with equivalent studies by other authors and show indications that assimilation of TPW will directly aid in improving the representation in the model of the boundary-layer thickness.

6. References

Alishouse, J.C., Snyder, S.A., Vongsathorn, J., and Ferraro, R.R., 1990, Determination of oceanic precipitable water from the SSM/I, IEEE Trans. Geosci. Remote Sensing, 28, 5, 811-816.

Bauer, P., and Schluessel, P., 1993, Rainfall, total water, ice water, and water vapour over sea from polarized microwave simulations and Special Sensor Microwave/Imager data, JGR, 98, p.20,737-20,760.

Boutin, J., and Etcheto, J., 1996, Consistency of Geosat, SSM/I, and ERS-1 global surface wind speeds - comparision with in situ data, J. Atmospheric and Oceanic Technology, 13, 183-197.

Deblonde, G., and Wagneur, N., 1997, Evaluation of global numerical weather prediction analyses and forecasts using DMSP special sensor microwave imager retrievals. Part 1. Satellite retrieval algorithm intercomparison study, Journal of Geophysical Research, 102, 1833-1850.

Deblonde, G., Yu, W., Garland, L., and Dastoor, A.P., 1997, Evaluation of global numerical weather prediction analyses and forecasts using DMSP special sensor microwave imager retrievals. Part 2. Analyses/forecasts intercomparison with SSM/I retrievals, Journal of Geophysical Research, 102, 1851-1866

Eyre, J.R., 1995, Variational assimilation of remotely-sensed observations of the atmosphere, Forecasting Research Division, Scientific Paper No.36

Fuhrhop,R., and Simmer, C., 1996, SSM/I brightness temperature corrections for incidence angle variations, Journal of Atmospheric and Oceanic Technology, 13, 1, 246-254.

Goodberlet, M.A. and Swift, C.T., 1992, Improved retrievals from the DMSP wind speed algorithm under adverse weather conditions, IEEE Trans. Geosci. Remote Sensing, 30, 5, 1076-1077.

Greenwald, T.J., Stephens, G.L., Vonder Haar, T.H., and Jackson, D.L., 1993, A physical retrieval of cloud liquid water over the global oceans using the Special Sensor Microwave/Imager observations, J. Geophys. Res., 98, 18471-18488.

Hollinger, J.P., Peirce, J.L., and Poe, G.A., 1990, SSM/I instrument evaluation, IEEE Trans. Geosci. Remote Sensing, 28, 5, 781-790.

Jackson, T.J., 1997, Soil moisture estimation using special satellite microwave/imager satellite data over a grassland region., Water Resources Research, 33, 6,1475-1484.

Ledvina, D.V. , and Pfaendtner, J., 1995, Inclusion of Special Sensor Microwave/Imager (SSM/I) total precipitable water estimates into the GEOS-1 data assimilation system, Monthly Weather Review, 123, 10, 3003-3015.

Nagler, T., and Rott, H., 1992, Development and intercomparisons of snow mapping algorithms based on SSM/I data, IGARSS'92 (1992,Houston), Volume 1. p.812-814

Penney, G., 1994, A sensitivity study of SSM/I statistical and Physical liquid water path algorithms using a radiative transfer model, Forcasting Research Division, Technical Report No. 110.

Phalippou, L., 1996, Variational retrieval of humidity profile, wind speed and cloud liquid-water path with the SSM/I: Potential for numerical weather prediction, Quart. J. Royal Met. Soc., 122, 530, p.327-355.

Phalippou, L., and Gerard, E., 1996, Study report to the European Space Agency on the use of precise microwave imagery in numerical weather prediction

Schulz, J., and Schluessel, P., 1993, Water vapour in the atmospheric boundary layer over oceans from SSM/I measurements, Int. J. Remote Sensing, 14, 15, 2773-2789

Sheu,R.-S., Curry,J.A., and Liu,G., 1996, Satellite retrieval of tropical precipitation using combined International Satellite Cloud Climatology Project DX and SSM/I, Journal of Geophysical Research, 101, D 16, 21291-21301.

Steffen,K., and Schweiger, A. 1991, NASA team algorithm for sea ice concentration retrieval from Defense Meteorological Satellite Program special sensor microwave imager: comparison with Landsat satellite imagery, Journal of Geophysical Research, 96, C12, 21971-21987.

Teng, W.L., Wang, J.R., and Doraiswamy, P.C., 1993, Relationship between satellite microwave radiometric data, antecedent precipitation index, and regional soil moisture, International Journal of Remote Sensing, 14, 13, 2483-2500.

Vesperini, M., 1996, Humidity in the ECMWF model: monitoring of operational analyses and forecasts using SSM/I observations, EUMETSAT/ECMWF Fellowship programme, Research Report No. 3.

7. Figure Captions

Figure 1. SSM/I scanning geometry (from Hollinger et al. 1990)

Figure 2. Total precipitable water, calculated using a regression algorithm (Alishouse et al. 1990)

Figure 3. Global total precipitable water (TPW). a). Background field from UM. b). Difference field (1DVAR - Background).

Figure 4. Zonal mean plots of TPW retrieval properties.

Figure 5. Scatterplots for TPW showing a). comparison of 1DVAR with the Alishouse regression retrievals, b). 1DVAR with the model background.

Figure 6. Global surface windspeed. a). Background field from UM. b). Difference field (1DVAR - Background).

Figure 7. Zonal mean plots of surface windspeed retrieval properties

Figure 8. Scatterplots for surface windspeed showing a). comparison of 1DVAR with the Goodberlet regression retrievals, b).1DVAR with the model background.

Figure 9. Global cloud liquid water (CLW). a). Background field from UM. b). Difference field (1DVAR - Background).

Figure 10. Zonal mean plots of SSM/I CLW retrieval properties

Figure 11. Scatterplots for CLW showing a). comparison of 1DVAR with Weng regression retrievals, b). 1DVAR with the model background.

Appendices

APPENDIX A: SSM/I Fields stored in the MetDB

Element name	Element Description	Units
STLT_IDNY	Satellite Identifier	code tbl
ORBT_NMBR	Orbit number	numeric
SCAN_LINE_NMBR	Scan line number	numeric
POINT_ON_SCAN_LINE	Position number along scan	numeric
YEAR	Year	year
MNTH	Month	month
DAY	Day	day
HOUR	Hour	hour
MINT	Minute	minute
SCND	Second	second
RCPT_YEAR	Time of receipt year	year
RCPT_MNTH	Time of receipt month	month
RCPT_DAY	Time of receipt day	day
RCPT_HOUR	Time of receipt hour	hour
RCPT_MINT	Time of receipt minute	minute

The following elements are for the A scan

LTTD	Latitude	degrees
LNGD	Longitude	degrees
SRFC_TYPE	Type of surface	code
BRGTS_TMPR_F19GHZ_V	Brightness temp 19 GHz V	K
BRGTS_TMPR_F19GHZ_H	Brightness temp 19 GHz H	K
BRGTS_TMPR_F22GHZ_V	Brightness temp 22 GHz V	K
BRGTS_TMPR_F37GHZ_V	Brightness temp 37 GHz V	K
BRGTS_TMPR_F37GHZ_H	Brightness temp 37 GHz H	K
BRGTS_TMPR_F85GHZ_V	Brightness temp 85 GHz V	K
BRGTS_TMPR_F85GHZ_H	Brightness temp 85 GHz H	K

The following elements are for B scan 1

LTTD_1	Latitude	degrees
LNGD_1	Longitude	degrees
SRFC_TYPE_1	Type of surface	code
BRGTS_TMPR_F85GHZ_V_1	Brightness temp 85 GHz V	K
BRGTS_TMPR_F85GHZ_H_1	Brightness temp 85 GHz H	K

The following elements are for B scan 2

LTTD_2	Latitude	degrees

LNGD_2	Longitude	degrees
SRFC_TYPE_2	Type of surface	code
BRGTS_TMPR_F85GHZ_V_2	Brightness temp 85 GHz V	K
BRGTS_TMPR_F85GHZ_H_2	Brightness temp 85 GHz H	K

The following elements are for B scan 3

LTTD_3	Latitude	degrees
LNGD_3	Longitude	degrees
SRFC_TYPE_3	Type of surface	code
BRGTS_TMPR_F85GHZ_V_3	Brightness temp 85 GHz V	K
BRGTS_TMPR_F85GHZ_H_3	Brightness temp 85 GHz H	K
YEAR_STRT_OF_ORBT	Start time of orbit (year)	year
MNTH_STRT_OF_ORBT	Start time of orbit (month)	month
DAY_STRT_OF_ORBT	Start time of orbit (day)	day
HOUR_STRT_OF_ORBT	Start time of orbit (hour)	hour
MINT_STRT_OF_ORBT	Start time of orbit (minute)	minute
SCND_STRT_OF_ORBT	Start time of orbit (second)	second
YEAR_END_OF_ORBT	End time of orbit (year)	year
MNTH_END_OF_ORBT	End time of orbit (month)	month
DAY_END_OF_ORBT	End time of orbit (day)	day
HOUR_END_OF_ORBT	End time of orbit (hour)	hour
MINT_END_OF_ORBT	End time of orbit (minute)	minute
SCND_END_OF_ORBT	End time of orbit (second)	second
YEAR_OF_ASCDG_MODE	Time of ascending mode(year)	year
MNTH_OF_ASCDG_MODE	Time of ascending mode(month)	month
DAY_OF_ASCDG_MODE	Time of ascending mode (day)	day
HOUR_OF_ASCDG_MODE	Time of ascending mode (hour)	hour
MINT_OF_ASCDG_MODE	Time of ascending mode(minute)	minute
SCND_OF_ASCDG_MODE	Time of ascending mode(second)	second

APPENDIX B: SSM/I biases

Table of SSM/I biases and errors (obs + RT) applied in 1DVAR

Channel	Bias (K)	RMS error (K)
19V	-1.55	2.0
19H	-1.60	2.0
22V	-1.06	2.0
37V	0.38	2.0
37H	-1.34	2.0
85V	2.20	3.0
85H	1.75	3.0

APPENDIX C: Output Parameters

Parameters contained within 1DVAR output file

TIMDEP	Integer	Time of data point as (hour*100) + minute
LAT	float	Latitude of data point (decimal degrees)
LON	float	Longitude of data point (decimal degrees)
QCFLAG	Integer	= 10 x Interations + 1000 x Simulations (required for minimization) + STYPE
IFAIL	Integer	Reason for termination of NAG descent routine, E04LBF. 0 = Normal exit 1 = Bounds exceeded 2 = Max number of iterations allowed has been exceeded. F(x) may have no minimum 3 = Failure to satisfy the convergence criteria 4 = Not used 5 = All Lagrange-multiplier estimates lie close to zero
JCOST	float	Value of the cost function
GRADNORM	float	not used, set to 0
TBOBS_U(7)	float	Values of the unmodified SSM/I brightness temperatures for each of the 7 channels (19v, 19h, 22v, 37v, 37h, 85v, 85h)
TBMOD(7)	float	Values of the brightness temperatures in the 7 channels after optimisation
TPWM	float	UM total precipitable water (kg/m**2)
TPW	float	Optimal total precipitable water (kg/m**2)
TPWALI	float	Alishouse regression derived TPW (kg/m**2)
WINDSPB	float	UM surface windspeed sqrt(u**2+v**2) m s^{-1}
WINDSP	float	Optimal surface windspeed m s^{-1}
WINDGOO	float	Goodberlet regression derived windspd m s^{-1}
CLWB	float	UM cloud liquid water path kg/m**2
CLW	float	Optimal cloud liquid water path kg/m**2
WNGCLW	float	Wang regression CLW path kg/m**2
RAIN_ALI	logical	Alishouse regression rain detected flag
SI_GRODY	float	Grody scattering index
STYPE	Integer	Surface type: 0= ocean, 1= land, 2= seaice
TPWBL1	float	Background upper boundary layer tpw
TPWBL2	float	Background middle boundary layer tpw
TPWBL3	float	Background bottom boundary layer tpw
TPWL1	float	Optimal upper boundary layer tpw
TPWL2	float	Optimal middle boundary layer tpw
TPWL3	float	Optimal bottom boundary layer tpw
COSTOBS	float	= sum over all chans (I) (TBOBS_U(I)-TBMOD(I))**2/SDE2(I) where SDE2 is the variance of the error of the obs + model as given in Appendix B

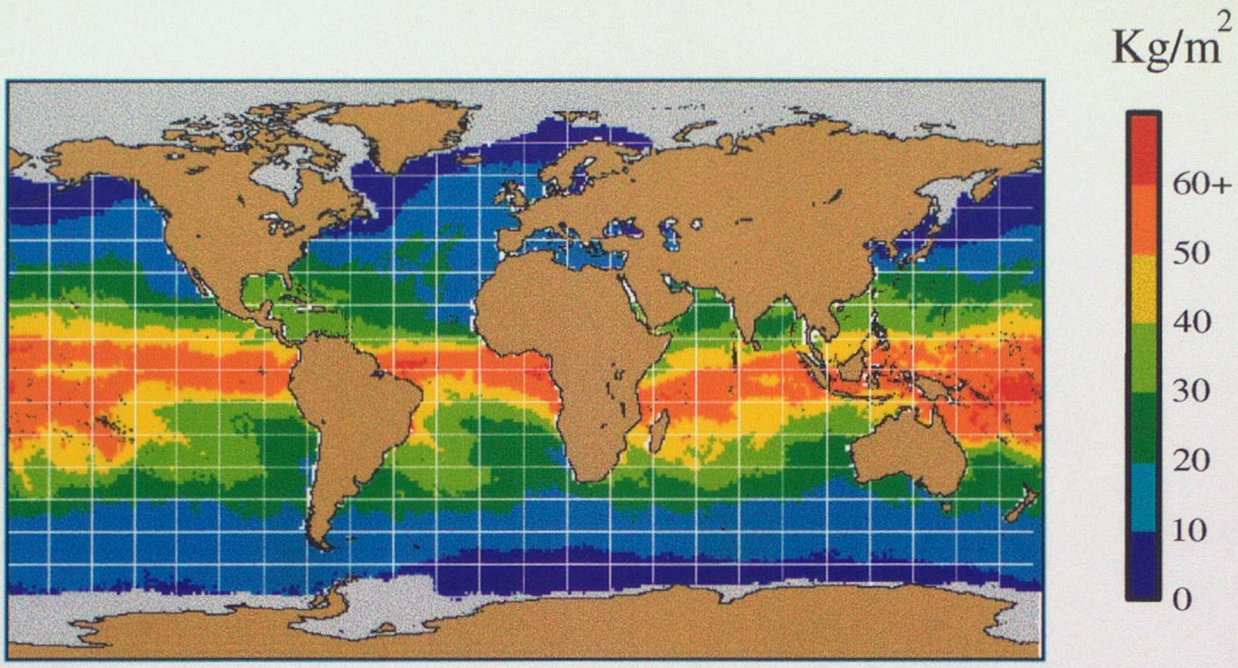

Figure 2. Total precipitable water, calculated using a regression algorithm (Alishouse et al., 1990)

a). Weekly average of Background TPW

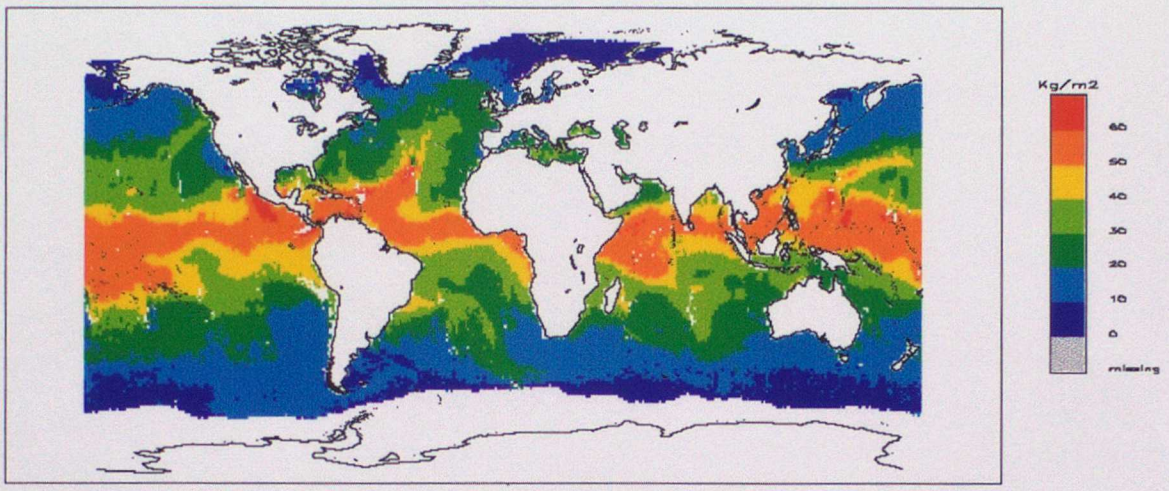

b). Weekly average TPW difference (1dvar - background)

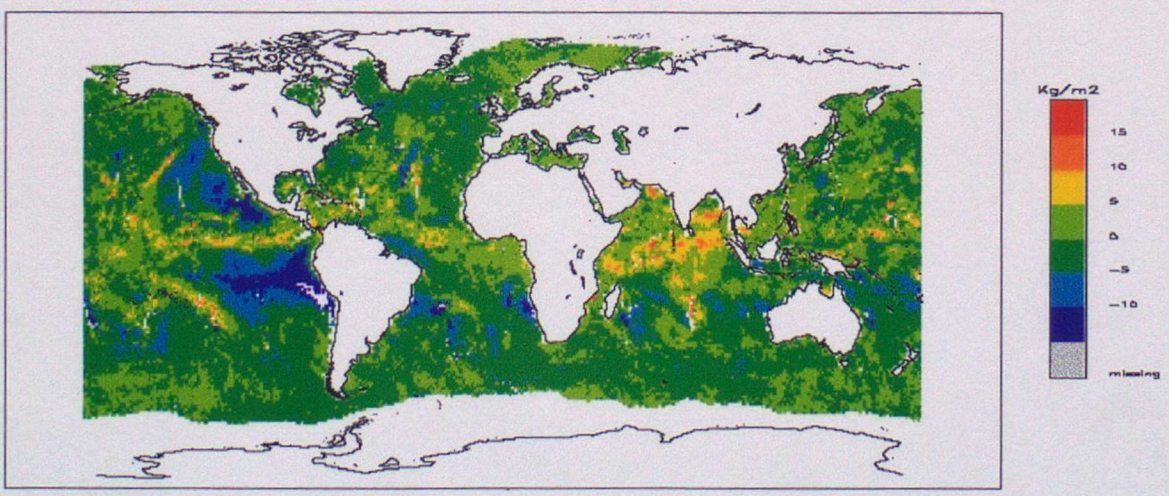

Figure 3. Global total precipitable water (TPW), a) Background field from UM and b) Difference field (1dvar - Background).

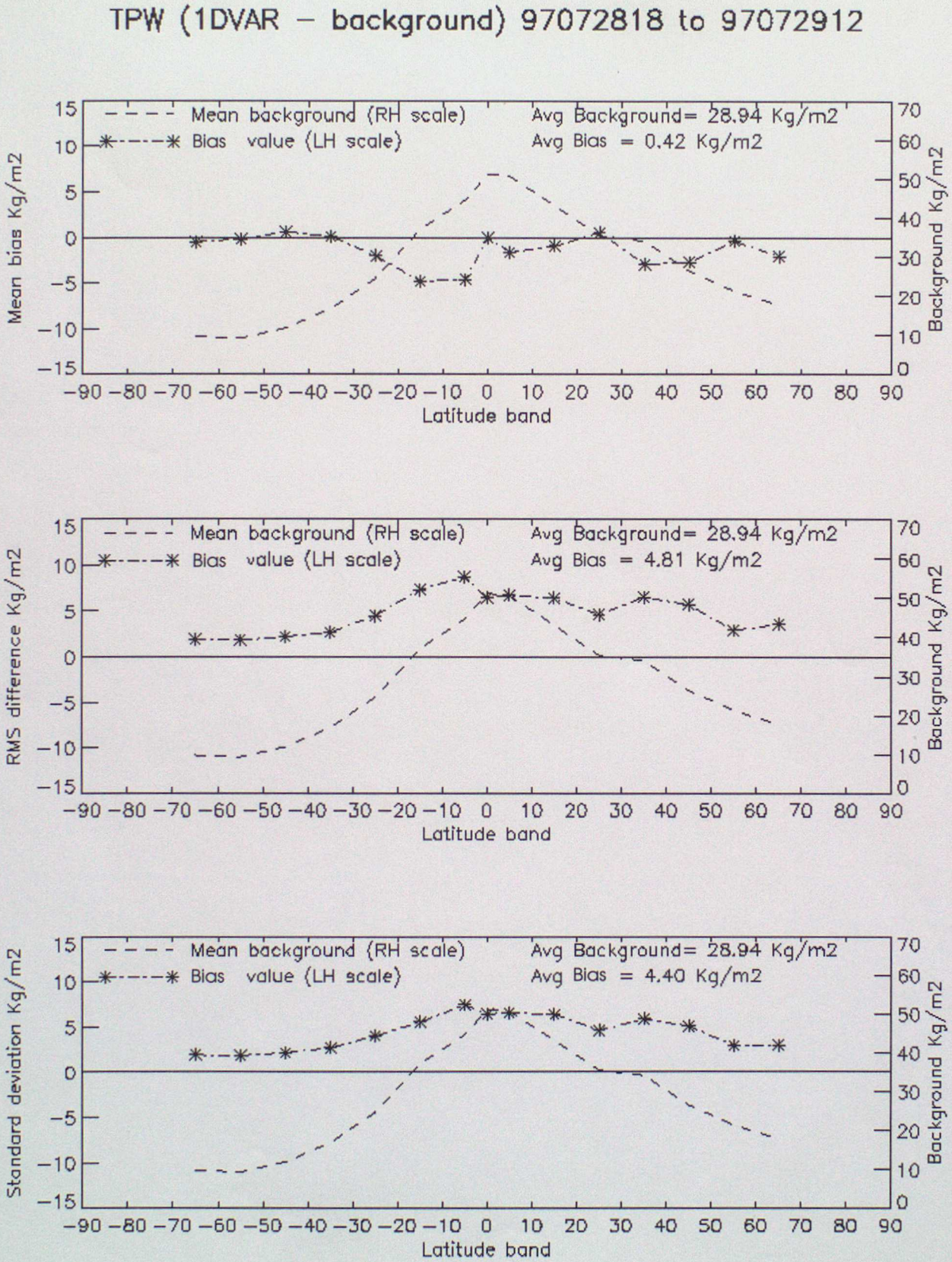

Figure 4. Zonal mean plots of SSM/I total precipitable water retrieval properties

a). Total Precipitable Water (precip. removed)

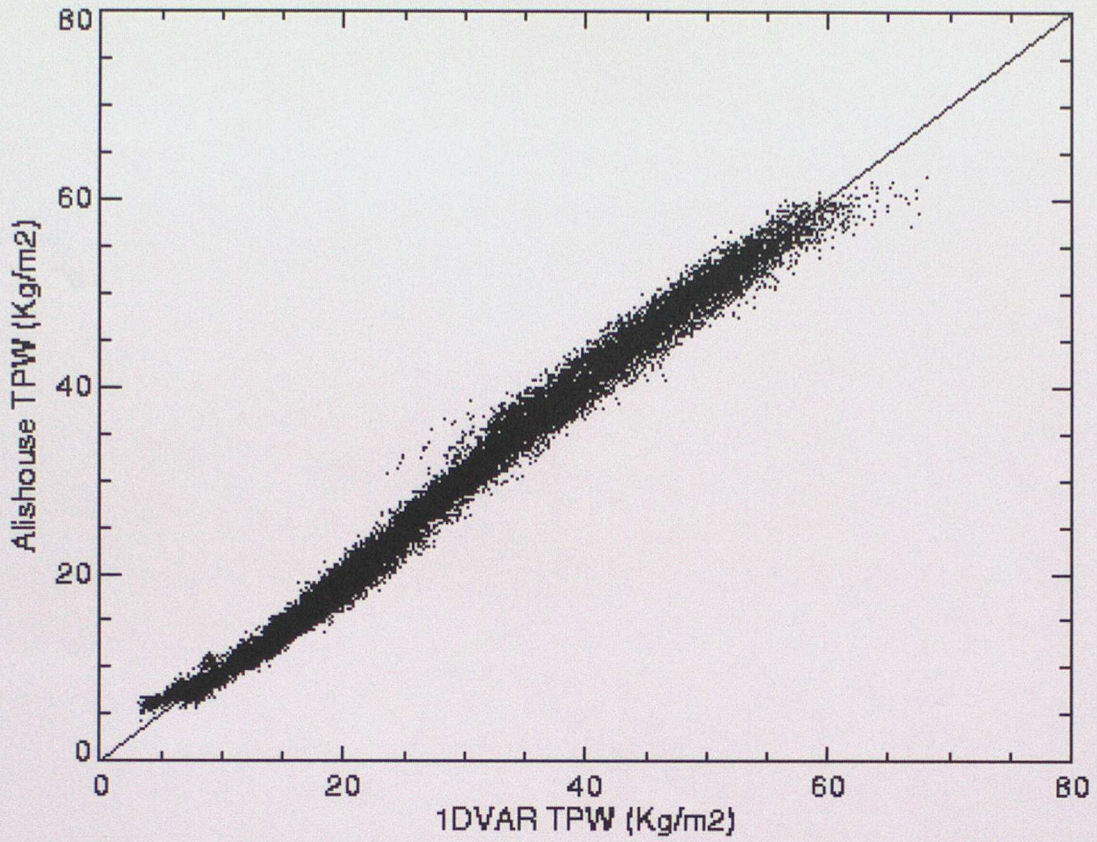

b).

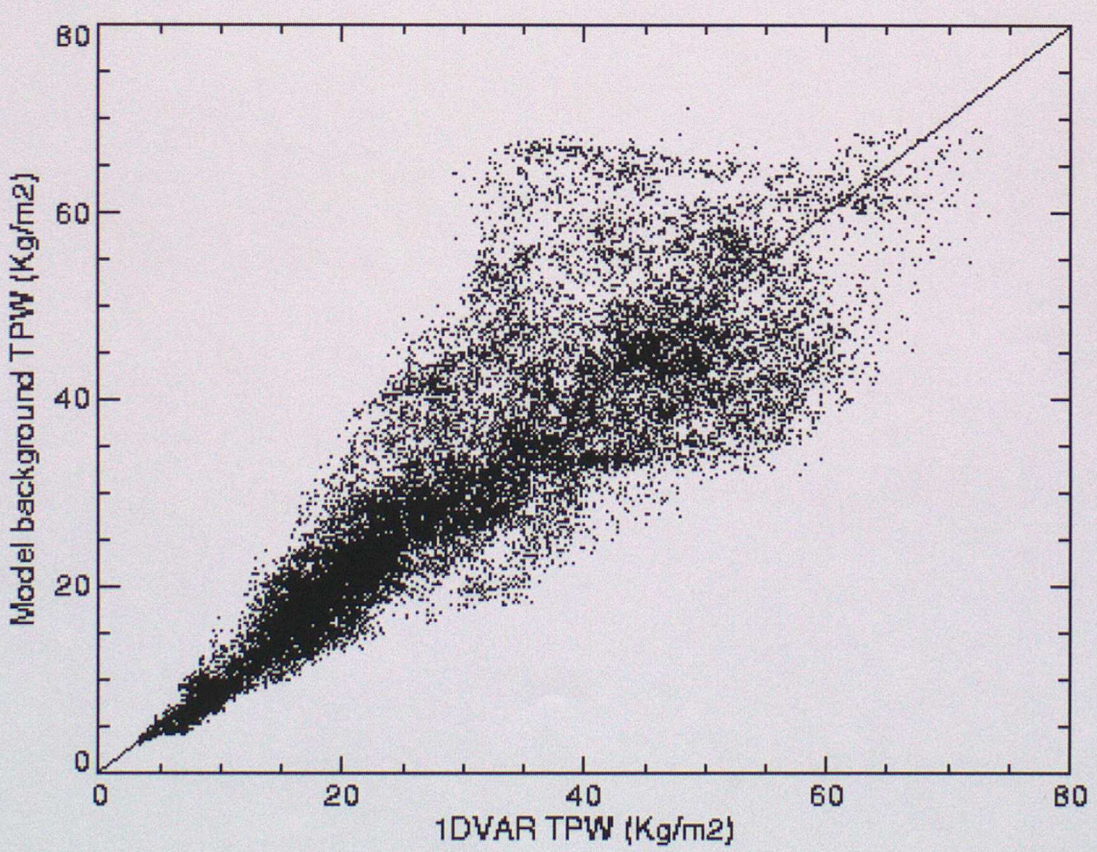

Figure 5. Scatterplots for TPW showing a) comparison of 1dvar with the Alishouse regression retrievals, b) 1dvar against the UM background.

a). Weekly average Background surface windspeed

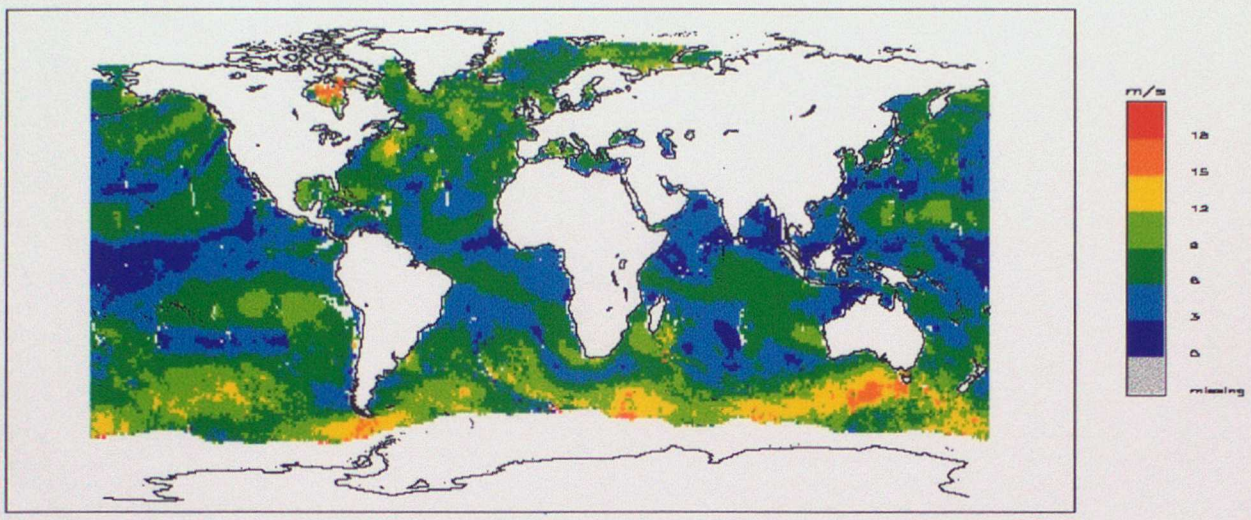

b). Weekly average windspeed difference (1dvar - Background)

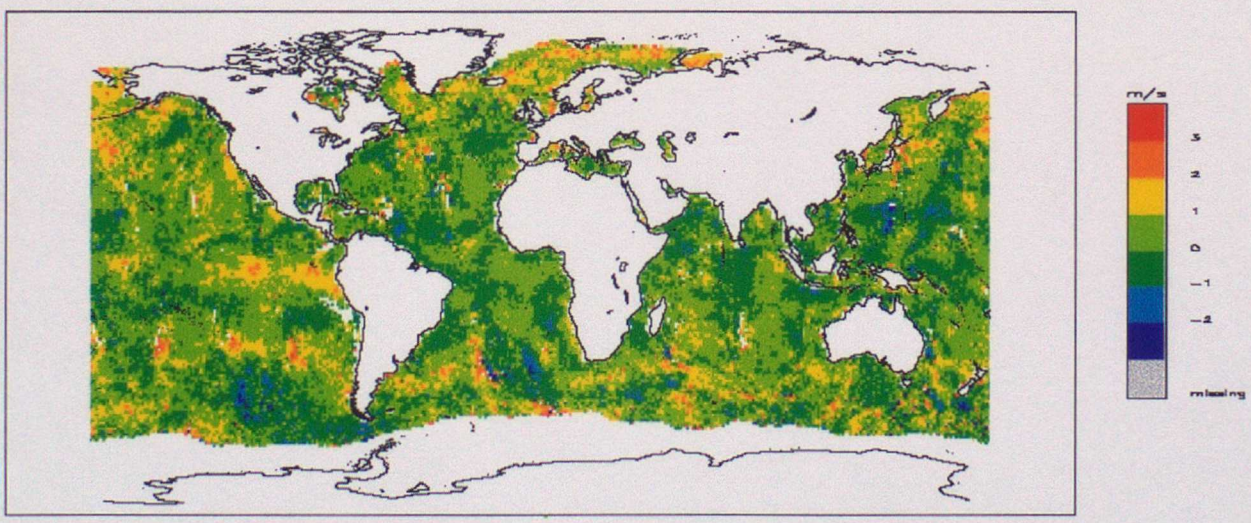

Figure 6. Global surface windspeed, a) Background field from UM and b) Difference field (1dvar - Background).

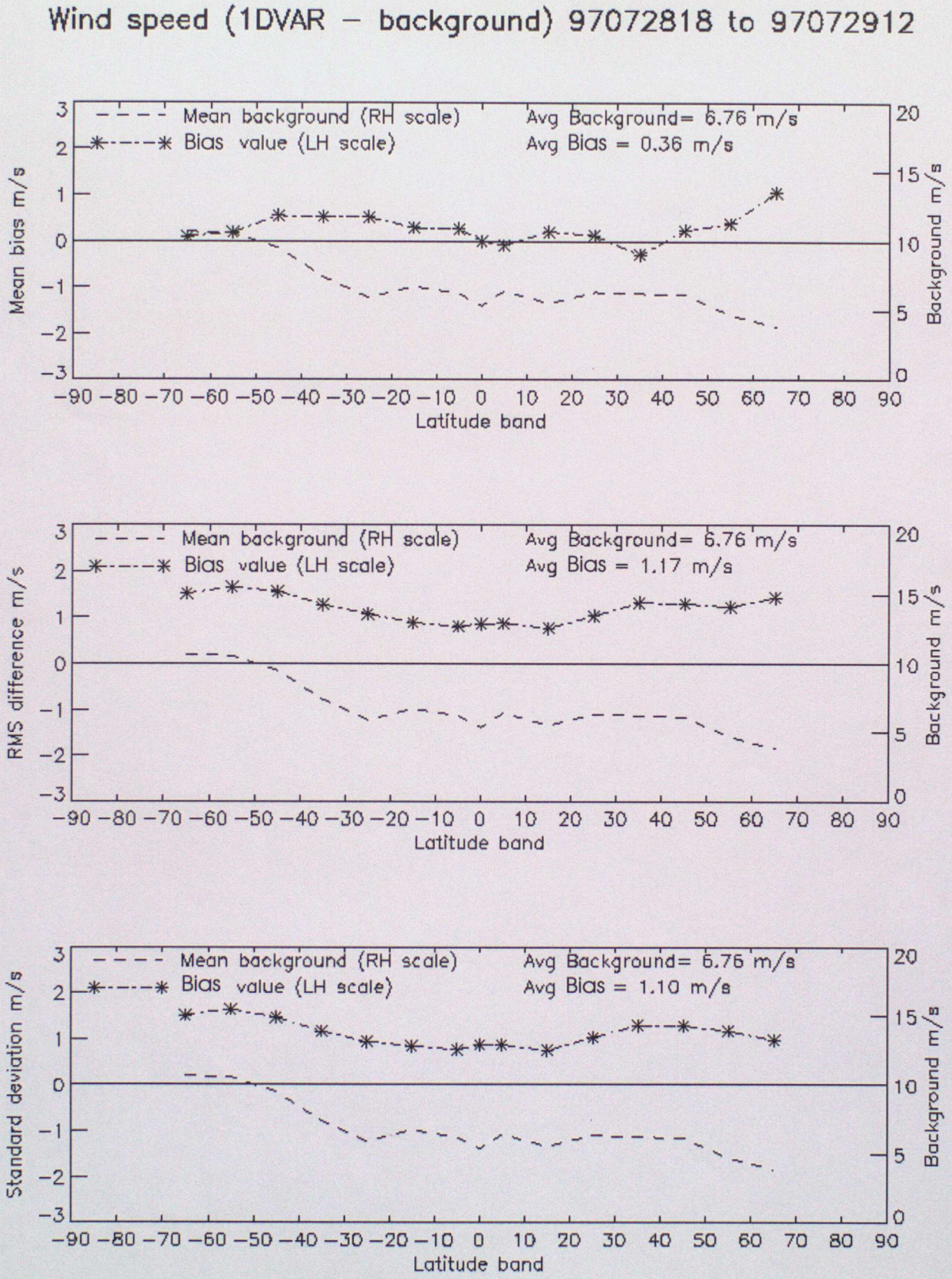

Figure 7. Zonal mean plots of surface windspeed retrieval properties

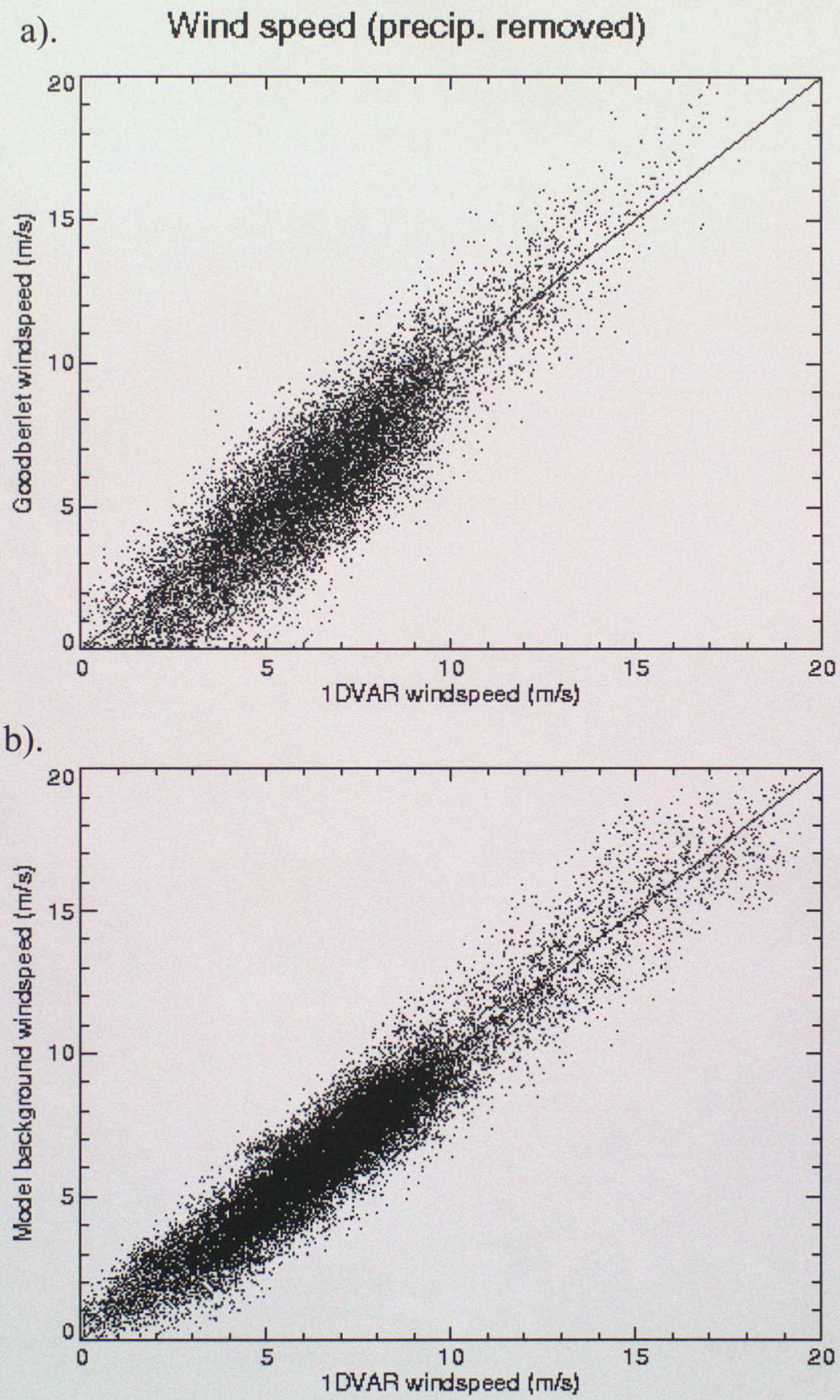

Figure 8. Scatterplots for surface windspeed showing a) comparison of 1dvar with the Goodberlet regression retrievals, and b) 1dvar with the UM background

a). Weekly average Background CLW

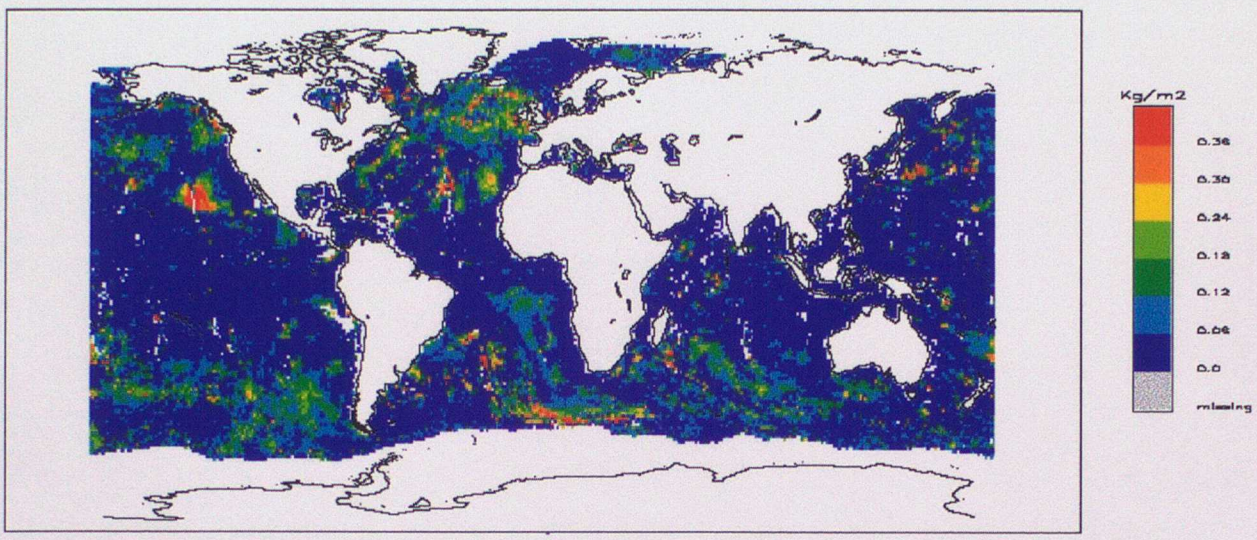

b). Weekly average CLW difference (1dvar - Background)

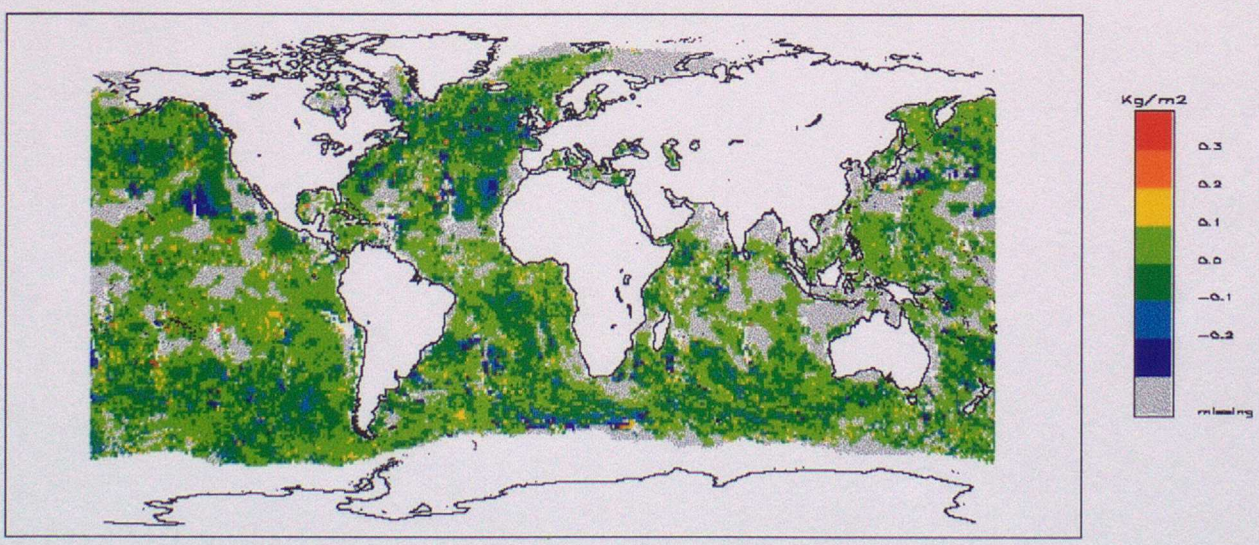

Figure 9. Global cloud liquid water (CLW), a) Background field from UM and b) Difference field (1dvar -Background)

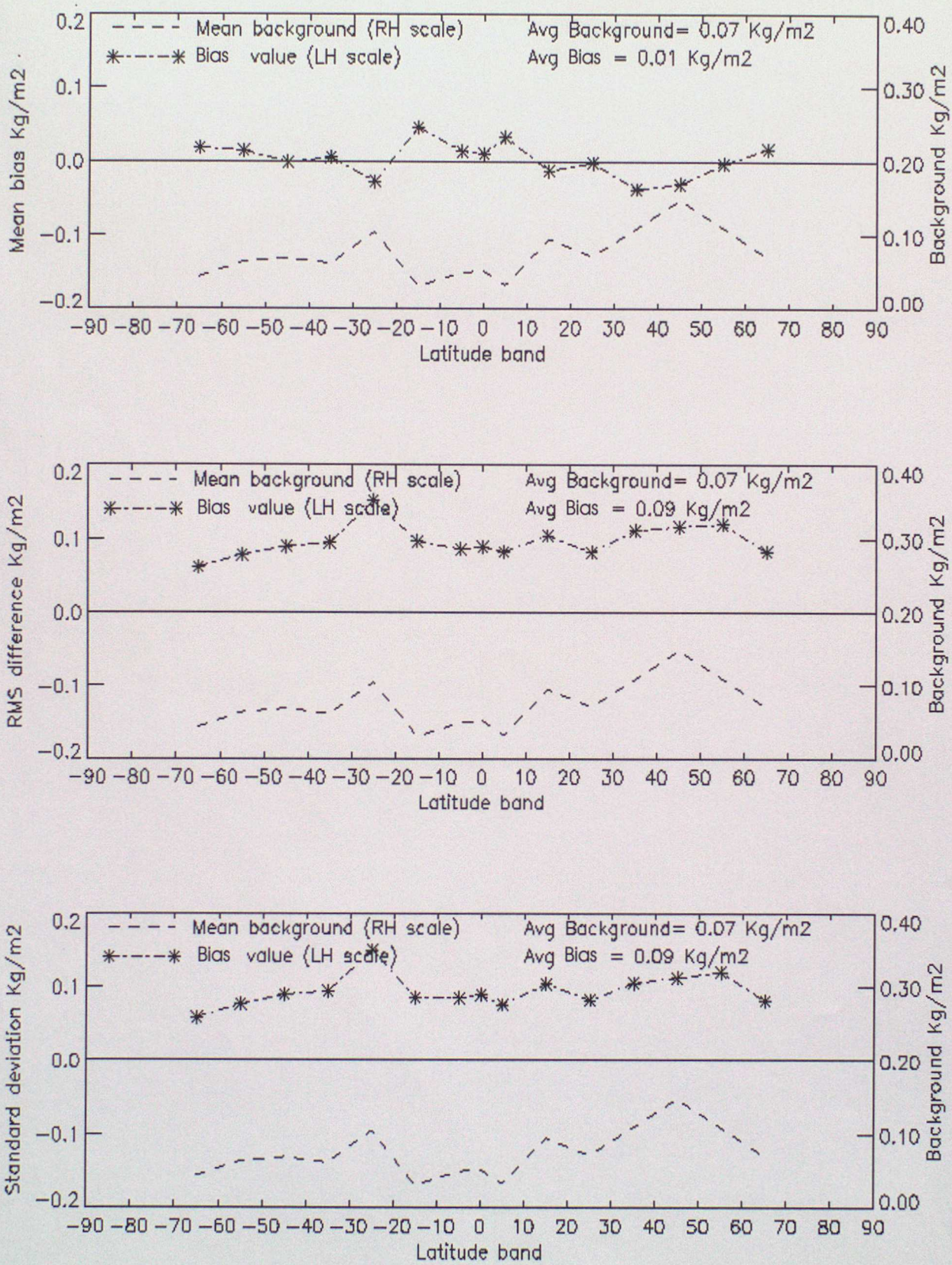

Figure 10. Zonal mean plots of SSM/I cloud liquid water retrieval properties

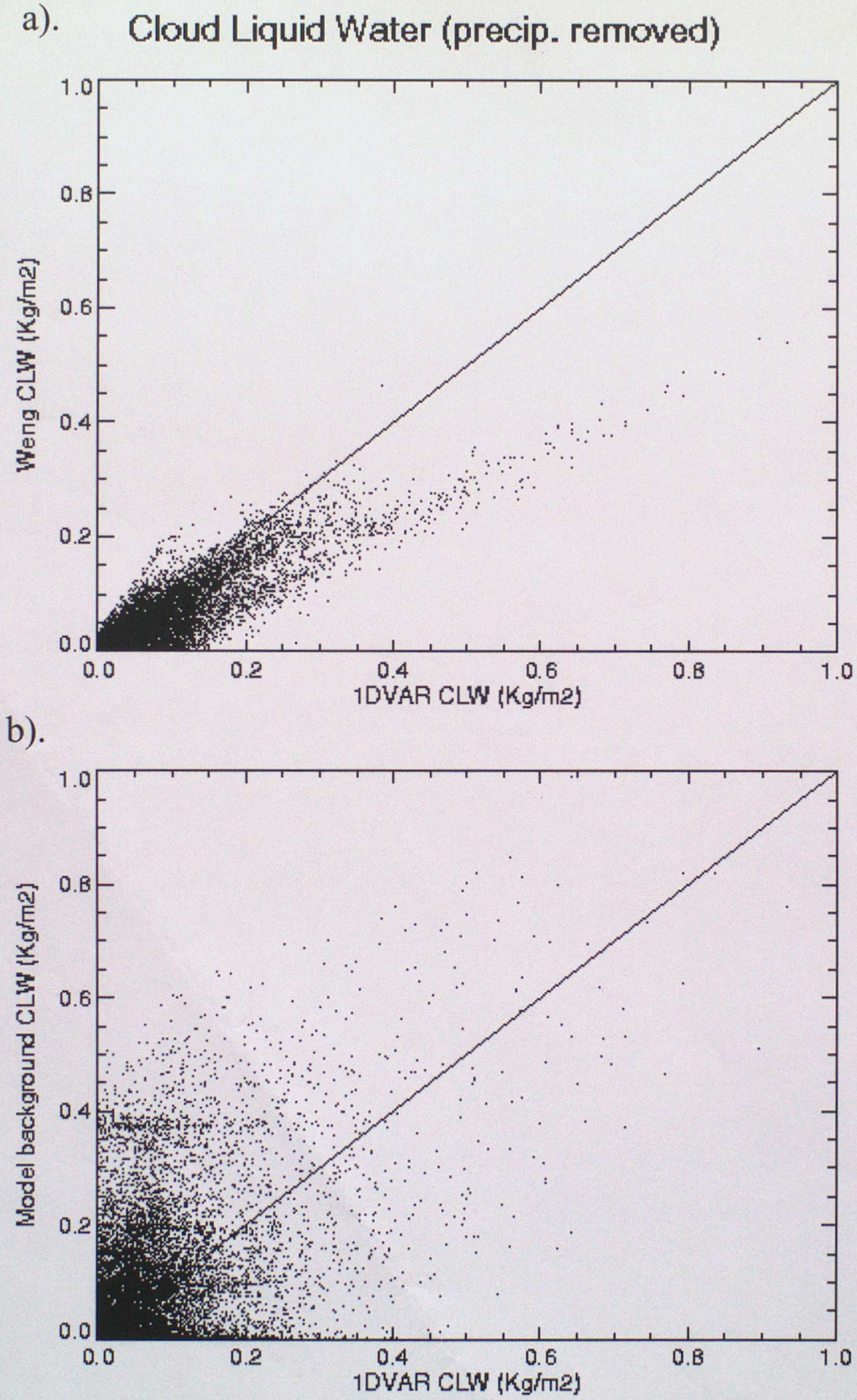

Figure 11. Scatterplots for CLW showing a) comparison of 1dvar with Weng regression retrievals and b) 1dvar with the UM background